

The effect of topography-enhanced diapycnal mixing on ocean and atmospheric circulation and marine biogeochemistry [☆]

T. Friedrich ^{a,*}, A. Timmermann ^a, T. Decloedt ^b, D.S. Luther ^b, A. Mouchet ^c

^a International Pacific Research Center (IPRC), SOEST, University of Hawai'i, Honolulu, HI 96822, USA

^b School of Ocean and Earth Science and Technology (SOEST), University of Hawai'i, Honolulu, HI 96822, USA

^c Département Astrophysique, Géophysique et Océanographie, Université de Liège, Liège, Belgium

ARTICLE INFO

Article history:

Received 17 July 2010

Received in revised form 18 April 2011

Accepted 30 April 2011

Available online 15 May 2011

Keywords:

Diapycnal mixing

Vertical diffusivity

Abysal circulation

Ocean ventilation

Oxygen minimum zones

ABSTRACT

The impact of topographically catalysed diapycnal mixing on ocean and atmospheric circulation as well as marine biogeochemistry is studied using an earth system model of intermediate complexity. The results of a model run in which diapycnal mixing depends on seafloor roughness are compared to a control run that uses a simple depth-dependent parametrization for vertical background diffusivity. A third model run is conducted that uses the horizontal mean of the topographically catalysed mixing as vertical profile in order to distinguish between the overall effect of larger diffusivities and the spatial heterogeneity of the novel mixing parametrization.

The new mixing scheme results in a strengthening of the deep overturning cell and enhances equatorial upwelling. Surface temperatures in the Southern Ocean increase by about 1 K (in the overall effect) whereas cooling of a similar magnitude in low latitudes is generated by the spatial heterogeneity of the mixing. The corresponding changes in the atmospheric circulation involve a weakening of the southern hemispheric Westerlies and a strengthening of the Walker circulation. Biogeochemical changes are dominated by an improved ventilation of the deep ocean from the south. Water mass ages decline significantly in the deep Indian Ocean and the deep North Pacific whereas oxygen increases in the two ocean basins. The representation of the global volume of water with an oxygen concentration lower than 90 $\mu\text{mol/kg}$ in the model is improved using the topography catalysed mixing. Furthermore, primary production is stimulated in equatorial regions through increased upwelling of nutrients and reduced in the oligotrophic gyres.

© 2011 Elsevier Ltd. All rights reserved.

1. Introduction

Observational studies indicate weak, O ($10^{-5} \text{ m}^2/\text{s}$), diapycnal mixing in the ocean's interior (Gregg, 1987; Kunze and Sanford, 1996; Kunze et al., 2006; Ledwell et al., 2011) and bottom-intensified mixing orders of magnitude larger in regions of rough topography (Gregg and Sanford, 1980; Toole et al., 1997; Polzin et al., 1997; Klymak et al., 2006; Aacan et al., 2006; Levine and Boyd, 2006). The diapycnal diffusivity, K_ρ , is therefore depth-dependent and patchily distributed in the horizontal in contrast to diffusivity parametrizations generally adopted in OGCMs, that often use horizontally homogeneous and vertically varying values for K_ρ (Bryan and Lewis, 1979).

A spatially varying mixing parametrization has been developed over the past decade by St. Laurent (1999), Jayne and Laurent (2001) and St. Laurent et al. (2002). This parametrization

represents the first attempt to capture the spatial distribution of diapycnal mixing resulting from the local dissipation of internal tides at generation sites and has been implemented in recent modeling studies (e.g., Simmons et al., 2004, Saenko and Merryfield, 2005, Koch-Larrouy et al., 2007, Jayne, 2009).

The observed bottom-intensification of diapycnal mixing in regions of rough topography is the result of a large number of topography-catalysed mixing processes. However, it remains unclear what fraction can be ascribed to the local dissipation of internal tides. Tentative energy budgets (Munk and Wunsch, 1998; Wunsch and Ferrari, 2004) suggest that the tides supply no more than half of the mechanical energy available for diapycnal mixing in the abyssal ocean. Interaction of non-tidal internal waves with topography may be equally important, through for example reflection off a sloping bottom at the critical frequency (Eriksen, 1998; Nash et al., 2004) and scattering off rough topography (Müller and Xu, 1992). The combination of tidal motions with near-inertial internal waves generated by storms has also been observed to lead to enhanced mixing (Aacan and Merryfield, 2008). In addition, abyssal mixing can be sustained by instability of internal lee waves associated with mesoscale near-bottom currents over rough topography (Polzin and Firing,

[☆] International Pacific Research Center contribution number 789; School of Ocean and Earth Science and Technology contribution number 8163.

* Corresponding author. Tel.: +1 808 9567385; fax: +1 808 956 9425.

E-mail address: tobiasf@hawaii.edu (T. Friedrich).

1997; Marshall and Garabato, 2008; Nikurashin and Ferrari, 2010), by hydraulic flow through constricted passages (Ferron et al., 1998; Thurnherr, 2006; St. Laurent and Thurnherr, 2007) and by episodic deep overflows (Lukas et al., 2001).

Dynamically, vertical gradients of the diapycnal diffusivity relate to the intensity of upwelling via the buoyancy equation and influence the horizontal circulation via vorticity dynamics (St. Laurent, 1999; Saenko and Merryfield, 2005). Circulation patterns calculated with spatially varying mixing can thus be expected to differ from those obtained with uniform mixing.

The sensitivity of the ocean circulation to the horizontal distribution of vertical mixing has been studied by a number of recent numerical studies (Hasumi and Suginoara, 1999; Simmons et al., 2004; Saenko and Merryfield, 2005; Emile-Geay and Madec, 2009; Jayne, 2009). In particular, horizontally non-uniform mixing has been shown to alter the abyssal circulation from the classical Stommel–Arons pattern (Huang and Jin, 2002; Katsman, 2006; Emile-Geay and Madec, 2009), to affect the deep ocean stratification (Hasumi and Suginoara, 1999; Saenko, 2006), to have a bearing on the depth and intensity of the Antarctic Circumpolar Current (Saenko and Merryfield, 2005; Jayne, 2009), as well as to yield improved temperature–salinity characteristics of simulated water masses (Simmons et al., 2004; Saenko and Merryfield, 2005; Koch-Larrouy et al., 2007). Zonally integrated quantities such as the meridional transport of heat and mass are found to be sensitive to the spatial distribution of diapycnal mixing in the deep Indian, Pacific and Southern Ocean basins (Saenko and Merryfield, 2005; Palmer et al., 2007) and down to thermocline depths in the Atlantic Ocean (Saenko and Merryfield, 2005; Griesel, 2005; Jayne, 2009).

Several studies have demonstrated the relationship between vertical mixing and biogeochemical parameters. Gnanadesikan et al. (2002) reported a doubling of new production in response to an increase of vertical diffusivity from 0.15 to 0.6 cm²/s in the upper 2000 m of the water column. As the driving forces behind this doubling the study identified the increase in convection and in vertical diffusive and advective fluxes. Furthermore it was found that the location where vertical mixing is increased appears to be crucial for the response of new production. Gnanadesikan et al. (2004) showed that changes in vertical diffusion lead to changes in the radiocarbon budget and the distribution of this tracer in the ocean. The advective surface flux of young water masses to the Southern Ocean as well as the influx into the tropics at depth were found to be strengthened by an increase in vertical diffusion. In the presentation of a global marine ecosystem model Schmittner et al. (2005) tested the model's performance under different vertical mixing parametrizations. They revealed a large sensitivity of chlorophyll concentration to the vertical mixing scheme in particular in low latitudes. It was also shown that the delicate balance of diffusion and upwelling which sets the depth of the nutricline is altered in response to a change in vertical diffusion which results in shallower (deeper) nutricline for higher (lower) values of mixing.

The effects of changes in the strength of the overturning circulation (which is directly connected to diapycnal mixing) on ocean biogeochemistry have been investigated in numerous studies. Schmittner et al. (2005) and Menviel et al. (2008b) reported a decrease in global primary production in response to a major weakening of the Atlantic Meridional Overturning Circulation (AMOC) which was mostly caused by a decrease in the supply of nutrients from the deep ocean. Schmittner et al. (2007), Schmittner and Galbraith (2008) and Okazaki et al. (2010) demonstrated the coupling of North Pacific ventilation to the state of the AMOC. In both studies an increase in subsurface oxygen levels was observed concordantly as a consequence of a weakened AMOC.

In our present study we incorporate an empirically-derived topography-catalysed diapycnal mixing scheme (Decloedt and Luther, 2010) describing the spatial distribution of the mean back-

ground diffusivity K_ρ resulting from a broad range of mixing processes into an earth system model of intermediate complexity. The model includes a three-dimensional global model of the marine carbon cycle, a terrestrial vegetation model, a sea ice model, an OGCM and a simplified 3 dimensional dynamical atmosphere. Through this approach we are able to study the potential impact of spatially non-uniform mixing on ocean circulation, climate and the carbon cycle. Our primary intention is to elucidate the effects topography-catalysed mixing on the different compartments of the Earth system as well as to study the interactions.

The paper is organized as follows: after the description of the earth system model and the experimental setup in Sections 2 and 3, respectively, we give a brief explanation of the roughness diffusivity model in Section 4. Section 5 presents and discusses our main results. We summarize our main findings in Section 6.

2. Model configuration

We use the Earth system model of intermediate complexity LOVECLIM (version 1.1) (Goosse et al., 2010; Menviel et al., 2008b) which is based on 5 coupled subsystems.

The sea ice-ocean component (CLIO) (Goosse et al., 1999) consists of a primitive equation ocean general circulation model with 3° × 3° resolution on a partly rotated grid in the North Atlantic. CLIO uses a free surface and is coupled to a thermodynamic–dynamic sea ice model (Fichefet and Morales Maqueda, 1997, 1999). In the vertical there are 20 unevenly spaced levels with a thickness ranging from 10 m near the surface to ~700 m below 3000 m. Mixing along isopycnals, as well as the effect of mesoscale eddies on transports and mixing and downsloping currents at the bottom of continental shelves are parametrized (Goosse et al., 2010). The different vertical mixing parametrizations employed in our study are described in the following two sections. Bering Strait is closed in our simulations which inhibits freshwater transport from the Pacific into the Arctic.

The atmosphere model (ECBilt) is a spectral T21 model, based on quasigeostrophic equations with 3 vertical levels and a horizontal resolution of about 5.625° × 5.625°. Ageostrophic forcing terms are estimated from the vertical motion field and added to the prognostic vorticity equation and thermodynamic equation. Diabatic heating due to radiative fluxes, the release of latent heat and the exchange of sensible heat with the surface are parametrized. The seasonally and spatially varying cloud cover climatology is prescribed in the ECBilt version employed here.

The ocean, atmosphere and sea ice components model are coupled by exchange of momentum, heat and freshwater fluxes. The hydrological cycle over land is closed by a bucket model for soil moisture and simple river runoff scheme. Due to the weakness of the tropical trade winds simulated by the model, the moisture transport from the Atlantic to the Pacific is underestimated. To generate an Atlantic salty enough for an Atlantic Meridional Overturning Circulation (AMOC), a correction for freshwater flux is prescribed redirecting 8–15% of precipitation over the Atlantic to the North Pacific.

The global dynamic terrestrial vegetation is modelled using VE-CODE (Brovkin et al., 1997). Annual mean values of precipitation and temperature are communicated to the vegetation from the atmospheric model. On the basis of these mean values the evolution of the vegetation cover described as a fractional distribution of desert, tree, and grass in each land grid cell is calculated once a year. In the current version, only land albedo (as seen by the atmospheric model) outside the icesheets is changed by VE-CODE. Other processes such as vegetation effects on evapotranspiration or surface roughness are neglected.

LOCH is a three-dimensional global model of the oceanic carbon cycle with prognostic equations for dissolved inorganic carbon, total alkalinity, phosphate, dissolved and particulate organic matter, oxygen and silicates (Goosse et al., 2010; Menviel et al., 2008a,b). The phytoplankton growth is a function of temperature, light and phosphate concentration. The sink term depends on grazing and mortality. Although phytoplankton biomass is a prognostic variable it is not subject to advective transports. Remineralization below the euphotic zone (0 – 120 m) is a function of oxygen concentrations. Anoxic remineralization can occur in oxygen-depleted areas but is less efficient. The export production is accompanied by the export of opal assuming a constant silicate-to-phosphate ratio. Furthermore CaCO_3 (calcite and aragonite) shells are formed as a function of phytoplankton growth. The dissolution of shells occurs in the deepest ocean layer. For CaCO_3 the dissolution rate depends on the calcite and aragonite saturation states. A constant rate is used for opal. The loss of alkalinity, carbon, phosphate and silicate that is associated with organic matter that is not remineralized and the shells that are not dissolved is compensated by river influx. A run-off mask for the main rivers of the world is used for this compensation. The surface partial pressure of CO_2 is computed from total alkalinity, dissolved inorganic carbon, temperature and salinity. The parametrization of the gas transfer velocity follows Wanninkhof (1992). In a version that allows for free CO_2 variability, the atmospheric CO_2 content is predicted for each ocean time step taking into account the air–sea CO_2 fluxes calculated by LOCH as well as the air–vegetation CO_2 fluxes provided by VECODE. LOCH is coupled to CLIO, using the same time step. Biogeochemical tracers that are subject to advection and mixing are advected and mixed using the same circulation field and mixing parameters, respectively as in CLIO. Water mass ages presented in this paper are based on an age tracer which is included in LOCH. The age tracer is initialized to be zero. At each time step the length of the time step is added except for the surface layer where the age tracer is restored to zero. The age tracer is subject to the same advection and horizontal and vertical mixing as all other tracers in LOCH.

A more detailed description of the LOCH model including the relevant equations for the evolution phytoplankton biomass and remineralization can be found in Goosse et al. (2010).

3. The 3-dimensional roughness diffusivity model

The mixing parametrization adopted in this study is the roughness diffusivity model (RDM) presented by Decloedt and Luther (2010). The premise of the RDM is that total topography-catalysed mixing can be approximated as depending mainly on topographic roughness. The functional form of the RDM is based on a heuristic recipe for the TKE dissipation rate profile resulting from the breaking of bottom-generated internal waves as a function of height h above bottom (Polzin, 1992, 2004). The RDM has the functional form:

$$K[h, r(x, y)] = K_b(r)[1 + h/h_0(r)]^{-2} + K_0 \quad (1)$$

where the boundary diffusivity $K_b(r)$ and decay scale $h_0(r)$ are simple functions of topographic roughness $r(x, y)$ that have been determined empirically from ~ 300 microstructure observations of TKE dissipation rates. Microstructure profilers measure the turbulent velocity shear on centimeter scales from which the TKE dissipation rate can be inferred. The microstructure surveys used in the construction of the RDM were conducted around the Fieberling Guyot seamount in the northeast Pacific, the Brazil Basin (on and off the Mid-Atlantic Ridge) and the Hawaiian Islands Ridge (French Frigate Shoals, Necker and Nihoa Islands and the Kauai Channel) (black crosses in Fig. 1a).

The minimum diffusivity $K_0 = 5.6 \cdot 10^{-6} \text{ m}^2/\text{s}$ is the diffusivity that can be sustained by the Garret–Munk internal wave field (Polzin et al., 1995) assuming a mixing efficiency of $\Gamma = 0.2$. The value of K_0 is lower than the often used background value of $\sim 10^{-5} \text{ m}^2/\text{s}$. Recent studies, however, show that diapycnal diffusivity can fall well below $\sim 10^{-5} \text{ m}^2/\text{s}$ and that our minimum diffusivity lies well within the boundaries of observations (Kunze et al., 2006; Ledwell et al., 2011).

The RDM parameters $r(x, y)$ and $h_0(r)$ are derived from the altimeter-derived seafloor topography of Smith and Sandwell (1997) with a resolution of 2 arc-minutes between 72°S – 72°N . The ocean component of LOVECLIM has a horizontal resolution of $3^\circ \times 3^\circ$. In order to incorporate the RDM, diffusivities are interpolated from the 2 arc-minute grid of the RDM onto the $3^\circ \times 3^\circ$ grid of CLIO by calculating mean values of the RDM for each CLIO grid cell. The topography-catalysed mixing scheme is available with a lower resolution of $0.5^\circ \times 0.5^\circ$ at: <http://www2.hawaii.edu/~decloedt/>.

4. Vertical mixing parametrizations and experimental setup

Three different parametrizations can contribute to the actual vertical diffusivity in the ocean component (CLIO) of LOVECLIM (Goosse et al., 2010). In turbulent regions, like the surface mixed layer, vertical diffusivity is proportional to the characteristic velocity and length scale of the turbulent motion. Here, the mixing parametrization is based on the Mellor and Yamada level 2.5 model (Mellor and Yamada, 1982), (see Goosse et al. (1999) for a detailed description). In addition vertical diffusivity is increased to $10 \text{ m}^2/\text{s}$ whenever the density stratification is unstable allowing for rapid stabilization of the water column. A background diffusivity is applied whenever the local diffusivity derived from the Mellor and Yamada scheme is lower than the local background diffusivity value which is mostly the case for deeper water layers of little turbulence outside the surface mixed layer. It is this background diffusivity that is different in our three model sensitivity simulations:

- In the case of the control run (**CTR-run**) this background diffusivity is simply depth-dependent and adapted qualitatively from the profile proposed by Bryan and Lewis (1979). In the deepest layer of our model, however, the diffusivity differs significantly from the “Bryan and Lewis”-profile. In combination with the parametrization of downsloping currents the values have been selected after a tuning in order to have the best possible water masses characteristics.
- The background diffusivity in the second run is based on the topography-enhanced RDM diffusivity scheme¹ which is explained in the previous section (**RDM-run**). Since the study by Smith and Sandwell (1997) does not provide bathymetry data poleward of 72° , the background diffusivity of the CTR-run was used to fill in data gaps.
- Our third model experiment uses the horizontal average of the RDM to prescribe a depth-dependent vertical diffusivity (**mean_{xy}(RDM)-run**). This allows us to discern between the effect of spatially-heterogeneous mixing and the overall effect of the new mixing parametrization where the latter is partly driven by simply higher diffusivity values throughout the water column.

All runs were integrated for more than 8000 years until a quasi-equilibrium in temperature, salinity, oxygen, phosphate, water mass age and dissolved inorganic carbon was reached in all deep ocean basins. The atmospheric CO_2 concentration was set to the

¹ $K[h, r(x, y)]$ in Eq. (1).

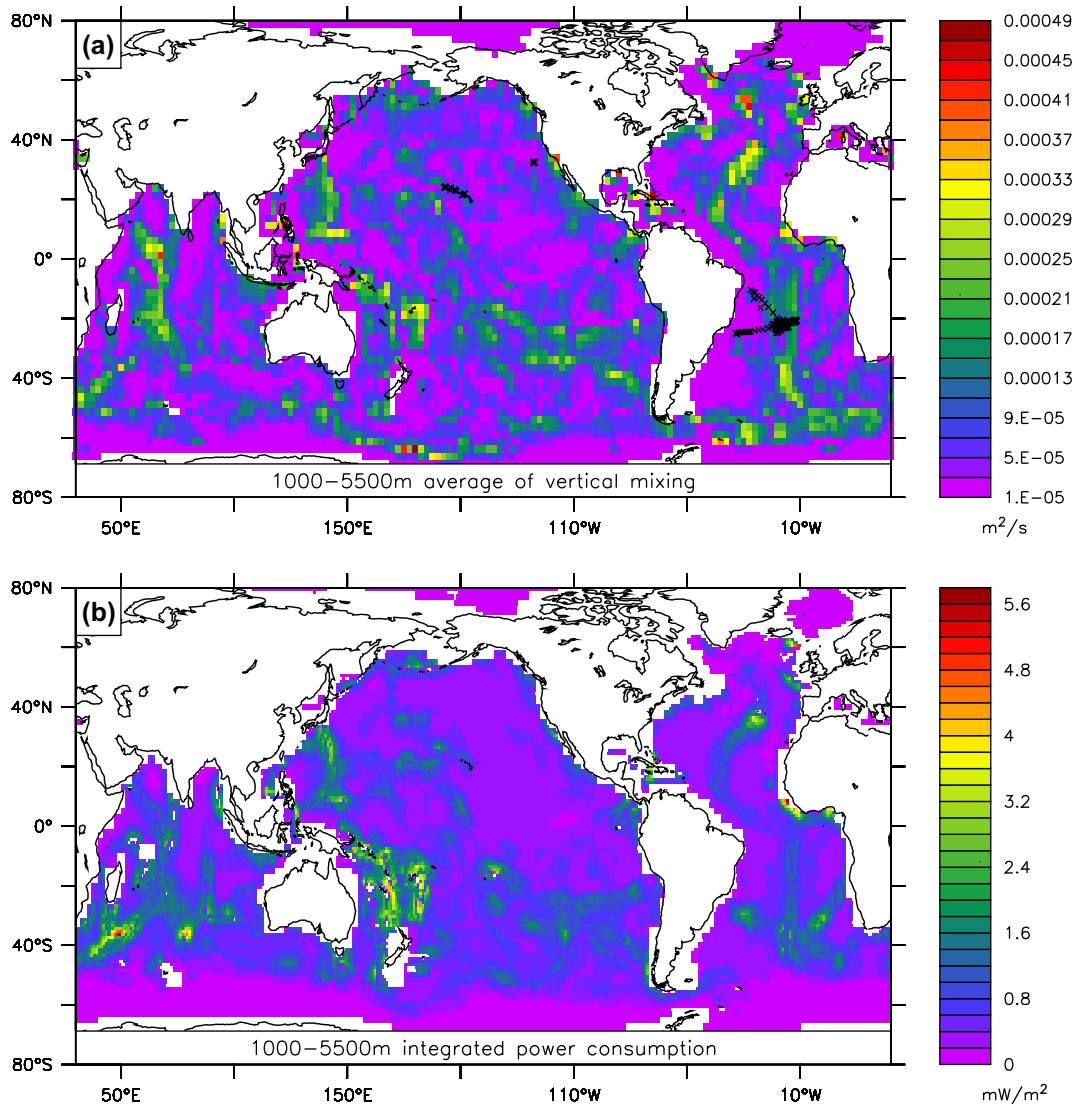


Fig. 1. (a): Average vertical diffusivity of the roughness diffusivity model (RDM) between 1000–5500 m in m^2/s . Black crosses indicate the locations of microstructure measurements used to derive the RDM. (b): Vertically integrated (1000–5500 m) power consumption in W/m^2 using Eq. (5) of Decloedt and Luther (2010). Values for potential density and buoyancy frequency were calculated using the Levitus climatology (Levitus, 1994).

preindustrial level of 280 ppmv during the integration. Subsequently the models were run for an additional 100 years with annual mean output. All numbers and figures presented in the study are based on averages over these 100 years.

5. Results and discussion

5.1. Changes in ocean and atmospheric circulation

The strength of vertical mixing arising largely from the topographic features varies by more than two orders of magnitude in the RDM. The lowest values of about $5 \cdot 10^{-6} \text{ m}^2/\text{s}$ are located at depths of 500–1000 m above the abyssal plains. Highest mixing rates reach $10^{-3} \text{ m}^2/\text{s}$ directly above ocean ridges and in the vicinity of fracture zones (Fig. 1a). The power consumed by this mixing scheme closely follows this patchy distribution (Fig. 1b).

Fig. 2 shows the horizontal averaged depth (potential density) profile of the three background diffusivity schemes used in this study. The largest differences between the two diffusivity parametrizations are found in the upper and lower thousand me-

ters of the water column. For the density classes between 23–27.6 kg/m^3 mixing rates are about twice as high for the RDM in the basin-mean than for the standard LOVECLIM. This results in a change of vertical density distribution. Compared to the control run (CTR-run) the top 300 m of the water column become denser in the RDM-run by up to 0.35 kg/m^3 . This increase is dominated by the equatorial regions where potential density of surface waters increases by about 1 kg/m^3 . Below 1700 m water becomes lighter by about 0.02 kg/m^3 . The overall effect is a global reduction in the stratification of the water column which is most pronounced in the near-surface waters around the equator. The three model simulations allow for differentiation between the overall effect of the new mixing parametrization and its heterogeneity effect. The overall changes (RDM-run–CTR-run) are not necessarily a direct consequence of enhanced bottom mixing but could also arise in response to higher values of vertical mixing. The RDM-run and the mean_{xy}(RDM)-run are using the same depth-profile of mixing. Thus, the heterogeneity effect of the topography-catalysed mixing scheme can be determined by their difference (RDM-run–mean_{xy}(RDM)). Comparing the mean vertical density distributions in the three runs (not shown) reveals that simulated near surface

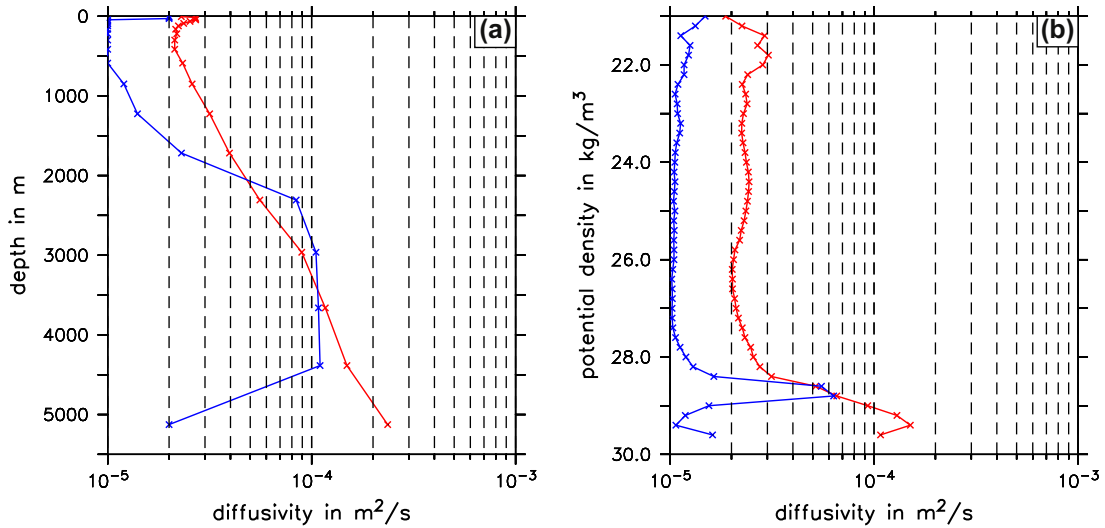


Fig. 2. Globally averaged vertical background diffusivity applied in the RDM-run (spatially-heterogeneous) and as a profile in the $\text{mean}_{xy}(\text{RDM})$ -run (red) and as applied in the CTR-run (blue) plotted versus depth (a) and potential density (b). Note the logarithmic x-axis in both plots. (For interpretation of the references to colour in this figure legend, the reader is referred to the web version of this article.)

density increase (0–200 m) in the RDM-run is mostly driven by the spatially-heterogeneous mixing. Below 1500 m, the RDM-run and the $\text{mean}_{xy}(\text{RDM})$ -run exhibit a similar mean vertical density profile. Thus, the decrease in deep ocean density is mostly due to higher vertical mixing values.

The second immediate consequence of stronger diapycnal mixing around topographic features in our simulation is an enhanced northward spread of deep and bottom waters formed in the Southern Ocean. Velocity anomalies below 3500 m between the RDM-run and the control run (Fig. 3a) and between the RDM-run and the $\text{mean}_{xy}(\text{RDM})$ -run (Fig. 3b) show a similar pattern in the Pacific

and the Indian Ocean with slightly larger anomalies in the overall effect. This indicates that the elevated northward flow is guided to a large extent by rough topography (and the associated increase in vertical mixing) such as the Tonga Trench, albeit the coarse resolution employed here. The effect of heterogeneous mixing around the Mid Atlantic Ridge is considerably smaller and only recognizable in higher latitudes.

Overall, northward velocities are 2–5 times higher close to topographic features which is associated with a spin-up of the deep overturning cell (Fig. 3c, d), most notably in the Pacific and the Indian Ocean. For the deep ocean the effect of the

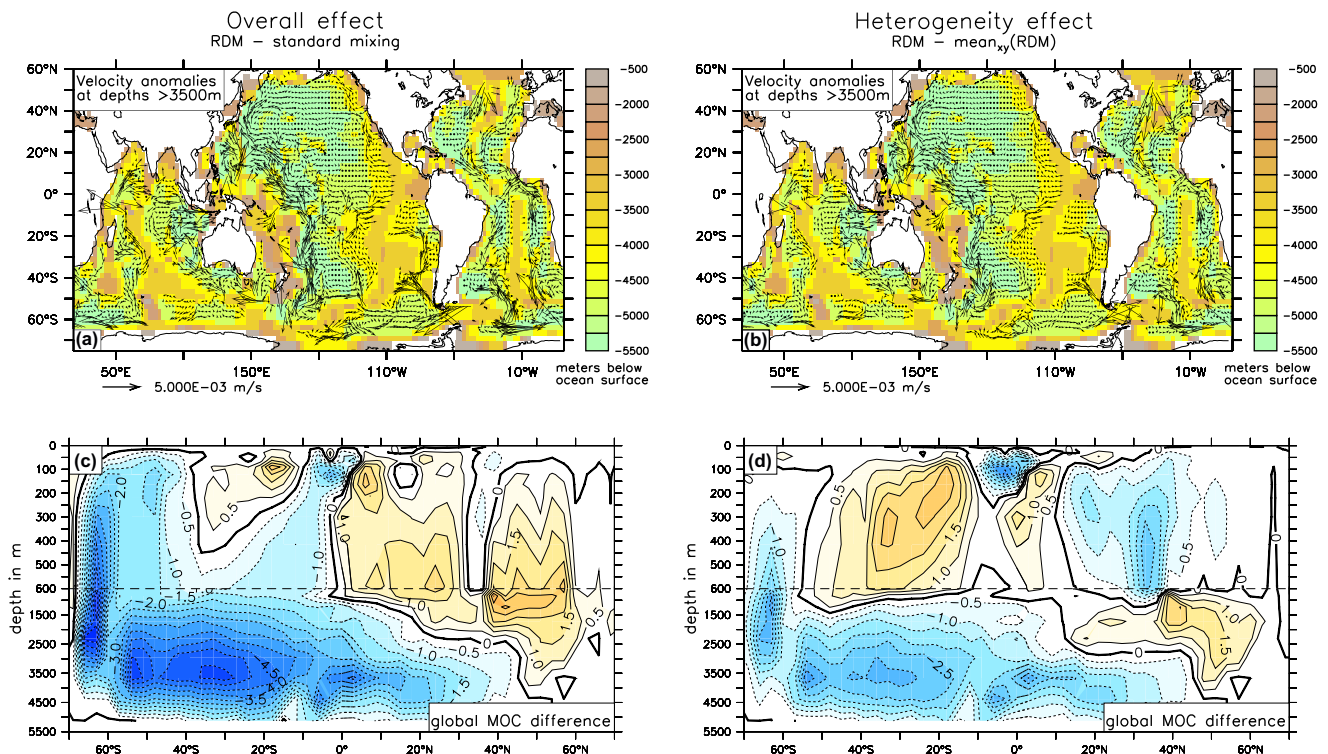


Fig. 3. Left panels (overall effect): (a): Model ocean topography (shaded) and difference in velocity (vectors) averaged over the lowest 3 depth levels (3300–5500 m) between the RDM-run and the control run. (c): Difference in Global Meridional Overturning Circulation in Sv ($1 \text{ Sv} = 10^6 \text{ m}^3/\text{s}$) between the RDM-run and the control run. Right panels (heterogeneity effect): same as left but for the difference between the RDM-run and the $\text{mean}_{xy}(\text{RDM})$ -run. Note the split z-axis in the panels c and d.

RDM on the global overturning is comparable to results of Emile-Geay and Madec (2009) (their Fig. 8c) who studied the impact of geothermal heating on ocean circulation. Both geothermal heating and rough seafloor topography are associated with seafloor spreading zones. Thus the spatial characteristics of enhanced mixing in both studies share similar features. But in addition to the mixing parametrization used in Emile-Geay and Madec (2009) that mostly affects the lowest water level, the RDM influences mixing in the entire water column which is accompanied by changes in ocean and atmospheric circulation on a nearly global scale. Comparing the global overturning anomalies in Fig. 3c, d demonstrates that about one half of the overturning increase in the deep ocean below 1500 m is driven by the patchy distribution of mixing whereas the other half can be attributed to larger mixing values. The largest differences between the overall and the heterogeneity effect can be found in upper water column of the Northern Hemisphere and are mostly caused by a different response of the North Pacific. Compared to the CTR-run, the RDM-run exhibits a basin-scale positive anomaly of in the meridional streamfunction of up to 2.5 Sv in the North Pacific reaching depth of up to 2000 m. This increase is not found for the RDM-run-mean_{xy}(RDM)-run anomalies and is thus not a consequence of spatially-heterogeneous mixing.

In conjunction with the spin-up of the bottom overturning cell, the upwelling in the Eastern Equatorial Pacific is also strongly amplified and slightly reduced in the western part (not shown) by the topography-catalysed mixing scheme. The eastward shift can be regarded as an effect of heterogeneous mixing. The strengthening of the upwelling in the Equatorial Pacific is partly driven by the anomalous North Pacific overturning. Therefore it is not as pronounced when comparing the RDM-run and the mean_{xy}(RDM)-run.

The overall changes (RDM-run-CTR-run) in the deep Indian Ocean are dominated by an increased influx of Antarctic Bottom Water (AABW). Below 3500 m enhanced northward flow along the South West Indian Ridge and the Mid Indian Ridge leads to an increased overturning cell in the deep ocean (not shown). The

change in the equatorial upwelling exhibits a similar pattern as in the Pacific with an increase (decrease) in the eastern (western) Indian Ocean (not shown). However, the magnitude in the Indian Ocean upwelling accounts only for about 50% of the increase simulated in the Pacific. When considering only the effect of heterogeneity, the magnitude of the changes is reduced by about 50% whereas the patterns are identical.

The effect of the new mixing parametrization on the Atlantic is also characterized by an enhanced inflow of AABW in the maximum density class originating near Antarctica along the western side of the Mid Atlantic Ridge (Fig. 3a, b). This results in a stronger northward flow of AABW into the North Atlantic as well as in a stronger recirculation into the eastern South Atlantic. The anomalous northward flow and recirculation is largely driven by higher mixing values and significantly smaller taking only the heterogeneity effect into account. However, the latter is responsible for an increase in the formation of North Atlantic Deep Water (the AMOC index increases by about 8%) and a strengthening of the shallow overturning cells and an associated increase in the upwelling in the equatorial Atlantic.

The changes in the deep circulation and the equatorial upwelling in the world's ocean are associated with large scale changes in surface ocean currents and temperature which in turn alters the atmospheric circulation pattern. The most prominent feature with regard to surface temperature is a cooling of the equatorial regions (Fig. 4a, b). The magnitude and pattern of this cooling is similar for both of the anomalies calculated from our model runs. Thus, we conclude that it is caused by the patchy distribution of the vertical mixing. Surface ocean temperature anomalies in the Southern Ocean are very different in our experiments. The overall effect is characterized by a significant warming which cannot be observed in the heterogeneity effect. Clearly, the Southern Ocean warming is the consequence of simply higher, global mean vertical diffusivities.

The changes in surface temperature can be mostly explained by the strengthening of the shallow and the deep overturning cells.

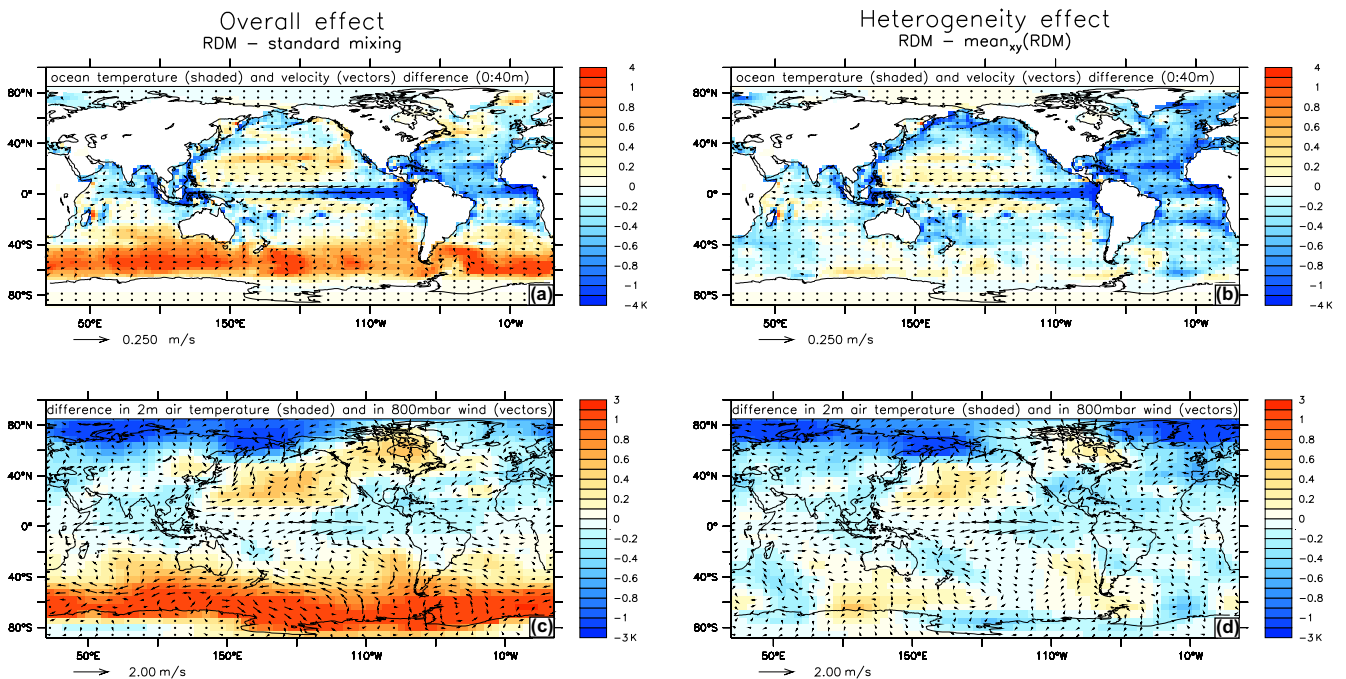


Fig. 4. Left panels (overall effect): (a:) Difference in ocean temperature in K (shaded) and velocity in m/s (vectors) averaged over the top 40 m between the RDM-run and the control run. (c:) Difference in 2 m air temperature (shaded) and 800 mbar wind velocity in m/s (vectors) between the RDM-run and the control run. Right panels (heterogeneity effect): same as left but for the difference between the RDM-run and the mean_{xy}(RDM)-run.

The increase in equatorial upwelling brings more cold water to the surface. In case of the overall effect, surface waters in the northern subtropical Pacific, the Labrador Sea and the Irminger Sea become slightly warmer. Here, the warming in northern hemispheric surface waters is caused by the slight increase in North Atlantic and North Pacific overturning respectively which strengthens the northward flow of warm waters. The same effect is responsible for the ~ 1 K warming of the Southern Ocean where the spin-up of the deep overturning cell is associated with an amplified southward transport of warm low-latitude waters that supplies the increased bottom water cell.

In addition, noteworthy is the cooling of surface waters along the western boundary of the Pacific and the Indonesian region. The topographic features incorporated in the RDM result in a significant strengthening of the boundary mixing leading to enhanced near coastal upwelling.

The surface salinity in the equatorial Pacific and the Indian Ocean is up to 0.5 psu higher in the RDM-run compared to the control run (up to 0.3 psu higher compared to the mean_{xy}(RDM)-run). This is a consequence of the increased upwelling in the eastern equatorial Pacific in conjunction with the atmospheric response to the cooling caused by it. In the case of a stronger upwelling the equatorial freshwater balance dominated by rainfall-driven dilution of horizontally and vertically advected water is shifted towards saltier conditions. In addition precipitation is reduced by up to 50% (RDM-run–CTR-run) over the areas that exhibit cooling due to increased upwelling. Thus, the upwelled water becomes saltier as it moves downstream towards the Indian Ocean.

Another atmospheric response in the equatorial Pacific is the strengthening of the Walker circulation, which in ECBilt is relatively weak. The increased upwelling in the east generates a zonal temperature gradient that leads to stronger equatorial easterly winds (Fig. 4c, d). A similar feature can be observed in the Indian Ocean. Thus, at the equator the response of the atmosphere to enhanced diapycnal mixing provides a positive feedback. Stronger winds induce stronger upwelling and increase the amount of sub-thermocline waters being brought back to the surface. The dipole pattern with warming of the subtropical surface waters in the North Pacific and cooling in the Atlantic is associated with a southerly wind anomaly over the North American continent which causes a warming of this area.

In accordance with studies by Saenko and Merryfield (2005) and Jayne (2009) we also find a strengthening of the Antarctic Circumpolar Current (ACC) and an associated increase of the transport through the Drake Passage. However, in the RDM-run Drake Passage transport increases by only about 7% compared to the CTR-run whereas Saenko and Merryfield (2005) report a 25% increase in the ACC. This discrepancy may have different reasons. Among them are differences in the mixing parameterization and in the mean model set-up. We speculate that this discrepancy could be at least to some extent caused by the windfield response to changes in the surface ocean temperature (which is not captured in the study by Saenko and Merryfield (2005)). The cooling of the tropics and the concurrent warming of the Southern Ocean result in a decrease of the meridional surface temperature gradient of 4% in the southern hemisphere. Fig. 4c shows that this leads to a weakening of the trade winds of 7% and the Westerlies of 5% around 40°S, respectively. The latter results in a weakening of the northward Ekman transport and thus a reduction of the meridional pressure gradient which partly drives the ACC. At this latitude we find eastward currents being reduced by 0.1–0.6 cm/s (not shown) in the depth range of 0–800 m. Between 45°S and 60°S we find a deep-reaching increase (0–2500 m) in the ACC of about the same magnitude. It is noteworthy that the Southern Ocean warming in our simulation is not solely caused by the strengthening of the deep overturning cell and the associated in-

crease in meridional heat transport. The warming provided by the latter entails a southward retreat of the sea-ice margin (defined as the position of the 0.15 m sea-ice thickness contour) of about 1° in the annual mean. This generates a positive feedback that further amplifies the warming due to a reduction in surface albedo. Overall the Southern Ocean warming strengthens the stratification in the upper 100 m between 40°S and 60°S by up to 100% which hampers convection and thus vertical mixing.

5.2. Changes in ocean biogeochemistry

Diapycnal mixing can alter ocean biogeochemistry in two ways. First of all, the distribution of relevant parameters such as nutrients, oxygen and dissolved inorganic carbon can be changed directly through mixing. In addition, the marine biogeochemistry is closely connected to the ocean physics through for example the ventilation of the abyssal ocean by horizontal advection, the upwelling of nutrients and the temperature dependencies of the solubility of oxygen and carbon dioxide.

The changes in the overturning and the upwelling in our simulation with topography-enhanced diapycnal mixing have a strong impact on the ventilation of the deep ocean (Fig. 5), the associated extension of the Oxygen Minimum Zones (Fig. 6c, d) and the primary production at low and mid-latitudes (Fig. 6a, b).

The anomaly pattern generated in the overall effect (RDM-run–CTR-run) in the Pacific and the Indian Ocean is dominated by a faster ventilation of the ocean at depths >1000 m through the increased deep overturning cell. Water mass ages drop locally by up to 500 yr in the western North Indian Ocean and by up to 700 yr in the western North Pacific (not shown). At the same time oxygen concentrations rise by 50–100 $\mu\text{mol/kg}$ at these locations (not shown). In the zonal-mean the age decreases by up to 100–300 yr (Fig. 5a, b). Oxygen levels increase by up to 50 $\mu\text{mol/kg}$ in the zonal-mean (Fig. 5c, d) due to the reduced time for remineralization to affect oxygen concentrations. The upper water column is characterized by a slight increase in water mass ages due to strengthening in the upwelling of “old” water. A similar dipole behavior of water mass ages in response to stratification was found by Gnanadesikan et al. (2007) (their Fig. 3 and 6d) and Oschlies et al. (2008) (their Fig. 5). Gnanadesikan et al. (2007) investigated the fate of ocean ventilation under global warming and the associated weakening of the overturning circulation. Our results support their suggestion that local water mass ages are the result of many different pathways to that point and are governed by an advection–diffusion balance.

Anomalies in deep ocean water mass ages and oxygen generated by the heterogeneity effect are about 50% smaller compared to the results seen in the RDM-run in accordance with smaller overturning anomalies. No increase in water mass ages is found in the sub-surface of the equatorial regions. Fig. 3d exhibits that the heterogeneity effect mostly causes a strengthening of the shallow overturning in this areas whereas the contribution of deeper (and “old”) water mass remains relatively unaltered.

The modifications induced by the RDM also alter the distribution of nutrients (phosphate in our model) in the surface ocean and thus the primary production (PP). The coupling of nutrient concentrations and PP to the overturning circulation state was already described by Schmittner (2005) and Menviel et al. (2008b). Both studies find that for a reduced AMOC near-surface nutrient concentrations and PP decrease in the equatorial Pacific. The results of our study confirm this coupling for an increased overturning. The topography-catalysed mixing results in lower phosphate concentration in the deep North Pacific (not shown) due to reduced residence time of the water. At the same time, subsurface waters in the equatorial Pacific are characterized by an increase in phosphate due to the strengthening in upwelling. However, in the euphotic

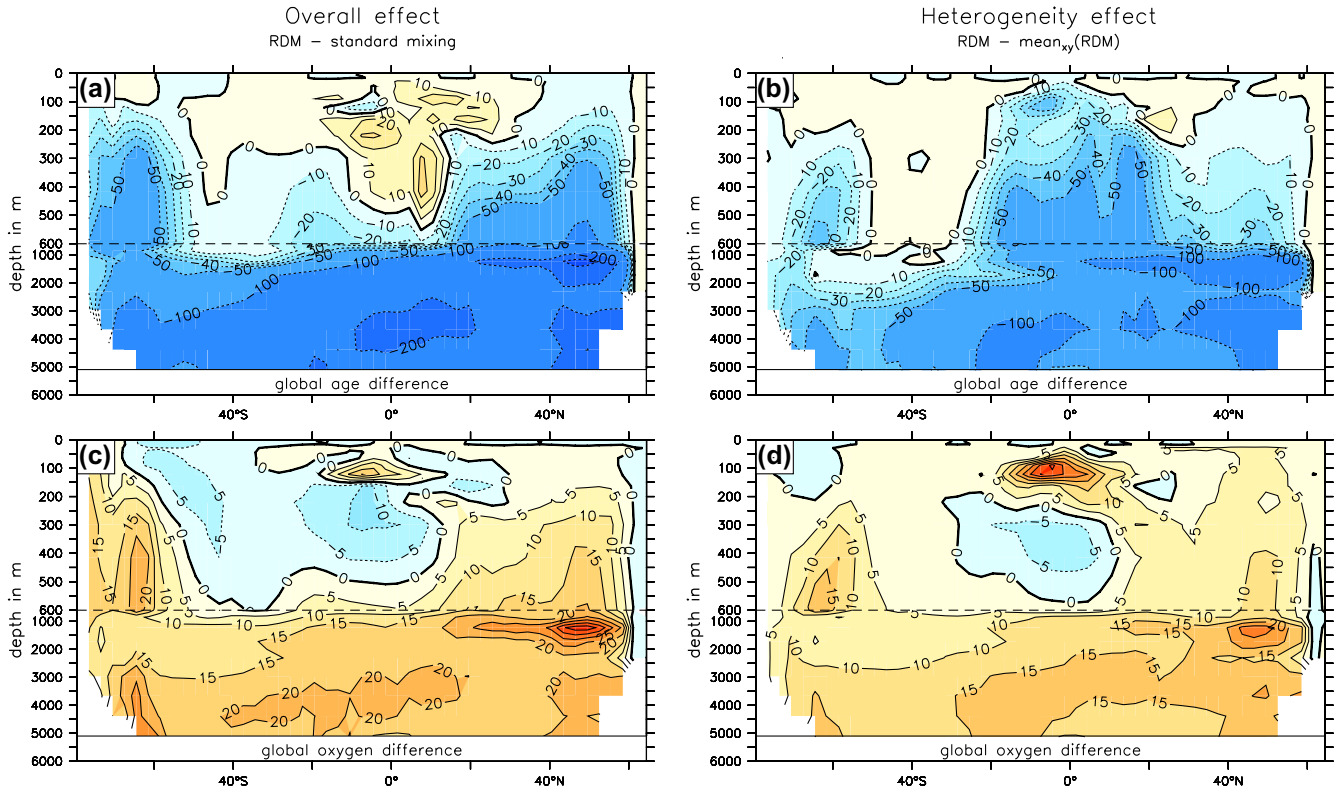


Fig. 5. Left panels (overall effect): Zonally averaged difference in water mass age in years (a) and Oxygen in $\mu\text{mol/kg}$ (c) between the RDM-run and the control run. Right panels (heterogeneity effect): same as left but for the difference between the RDM-run and the $\text{mean}_{xy}(\text{RDM})$ -run. Note the split z-axis in the plot.

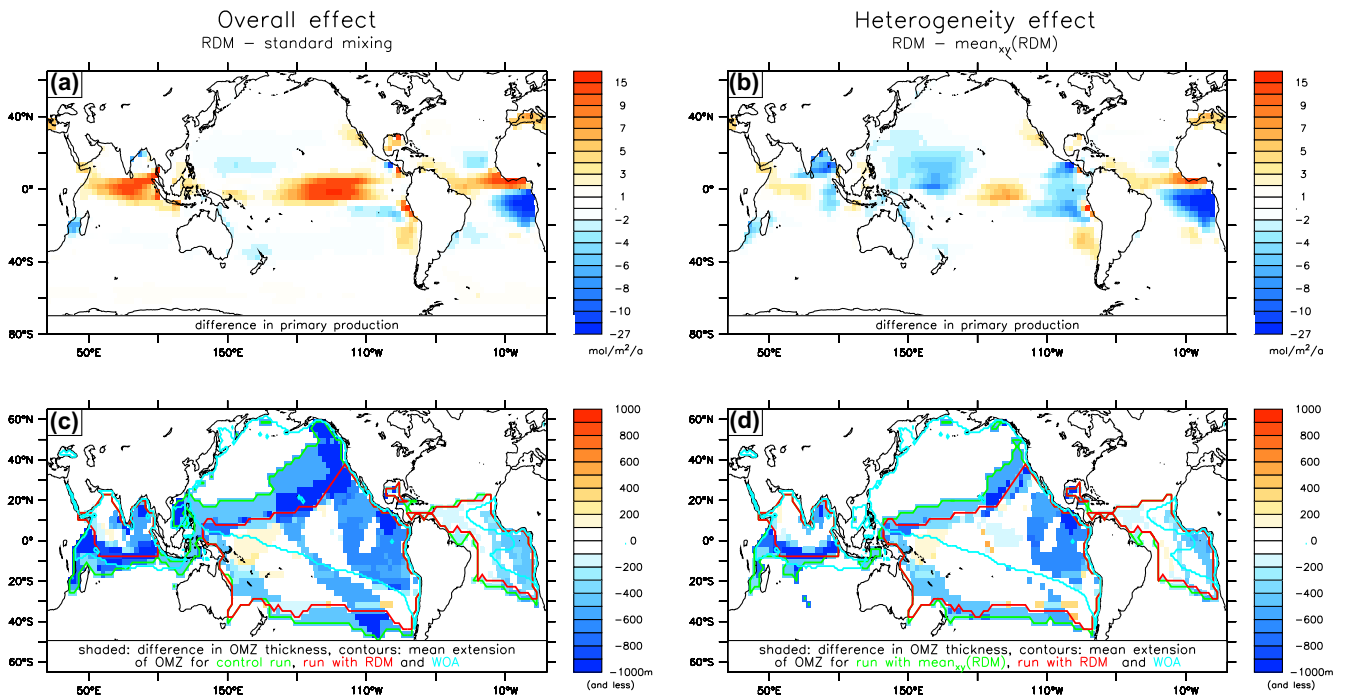


Fig. 6. Left panels (overall effect): (a) Difference in annual mean primary production in $\text{mol/m}^2/\text{a}$ between the RDM-run and the control run. (c) Difference in the thickness of the Oxygen Minimum Zone (defined as $\text{O}_2 < 90 \mu\text{mol/kg}$) between the RDM-run and the control run. Contours in (c) indicate the mean extension of the Oxygen Minimum Zone ($\text{O}_2 < 90 \mu\text{mol/kg}$) for the control run (green), the RDM-run (red) and World Ocean Atlas (cyan). Right panels (heterogeneity effect): same as left but for the difference between the RDM-run and the $\text{mean}_{xy}(\text{RDM})$ -run. (For interpretation of the references to colour in this figure legend, the reader is referred to the web version of this article.)

zone the response is different for the overall and the heterogeneity effect. On the one hand the strengthening in overturning and equatorial upwelling is weaker if only the effects of a patchy mixing dis-

tribution are taken into account (RDM-run- $\text{mean}_{xy}(\text{RDM})$ -run). On the other hand the pathway of water upwelling in the Pacific is different redirecting a large share of the deep water to the Southern

Ocean (Fig. 3c, d). This has a bearing on the response of PP to the new mixing parametrization. Fig. 6a shows that in case of the overall effect, PP is strongly increased near the equator and in the eastern Pacific coastal upwelling regions and decreased in the subtropical gyres and off the coast of Angola. The heterogeneity effect generates a similar pattern but of smaller magnitude in the Pacific (Fig. 6b).

As mentioned in Section 5.1, the upwelling shifts eastward in the equatorial Pacific. Accordingly the maximum growth in PP is found slightly west of the new upwelling center. The shift in upwelling has also an impact on the PP in the North Pacific subtropical gyre. The nutrient supply in this oligotrophic region is mostly provided by horizontal advection from high and low latitudes. Due to the eastward shift in the upwelling less phosphate can recirculate north at the western boundary as most of it is already utilized on the way across. On the other hand, water being brought back to the surface in the North Pacific by convection

and diapycnal mixing is now significantly younger (Fig. 5a, b) and thus less enriched in phosphate by remineralization.

The decline in PP seen in the overall effect in the southern hemispheric oligotrophic gyres is to a large extent caused by the Southern Ocean warming. The strengthening in surface stratification between 40°S and 60°S hampers the upward transport of nutrient-rich waters and with it the supply for the gyres through northward advection.

The changes in the eastern-equatorial PP in the Atlantic are a consequence of the northward shift in the tropical upwelling. Vertical advection of phosphate is increased (decreased) by up to 100% north (south) of the equator. Comparing the numbers in Fig. 6a it must be emphasized that even though changes in the subtropics appear to be small compared to the ones at the equator, they can account for 30–50% of the PP in the oligotrophic gyres. The relative increase in PP at the equator amounts to 50–150%. On a global scale simulated PP amounts to 57 GtC/yr in the CTR-run, 59 GtC/

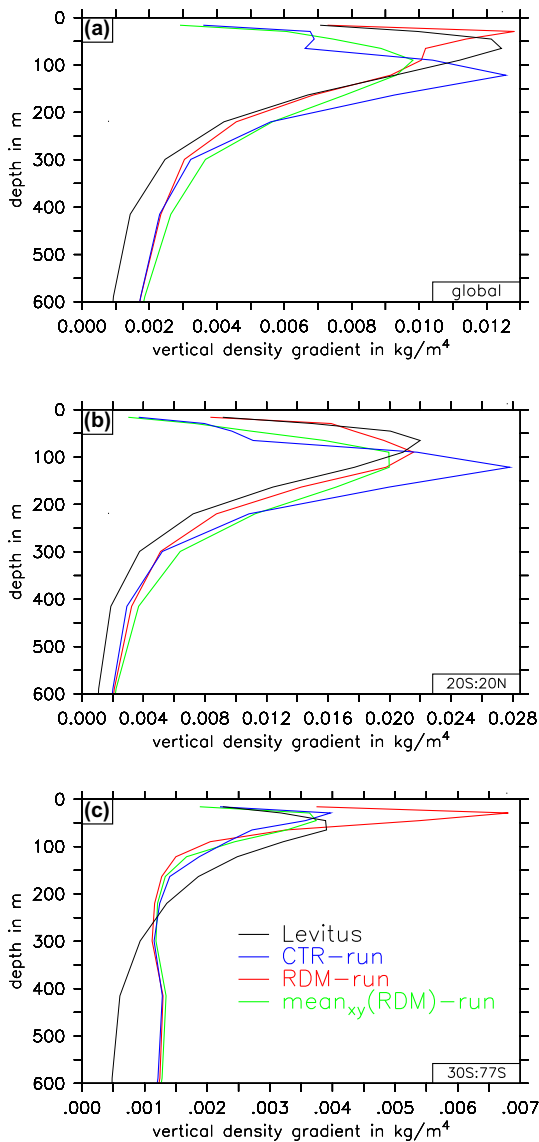


Fig. 7. Vertical density gradient in kg/m⁴ for the control run (blue), the RDM-run (red), the mean_{xy}(RDM)-run (green) and Levitus climatology (black) averaged globally (a), over 20°S to 20°N (b) and over 30°S to 77°S (c). (For interpretation of the references to colour in this figure legend, the reader is referred to the web version of this article.)

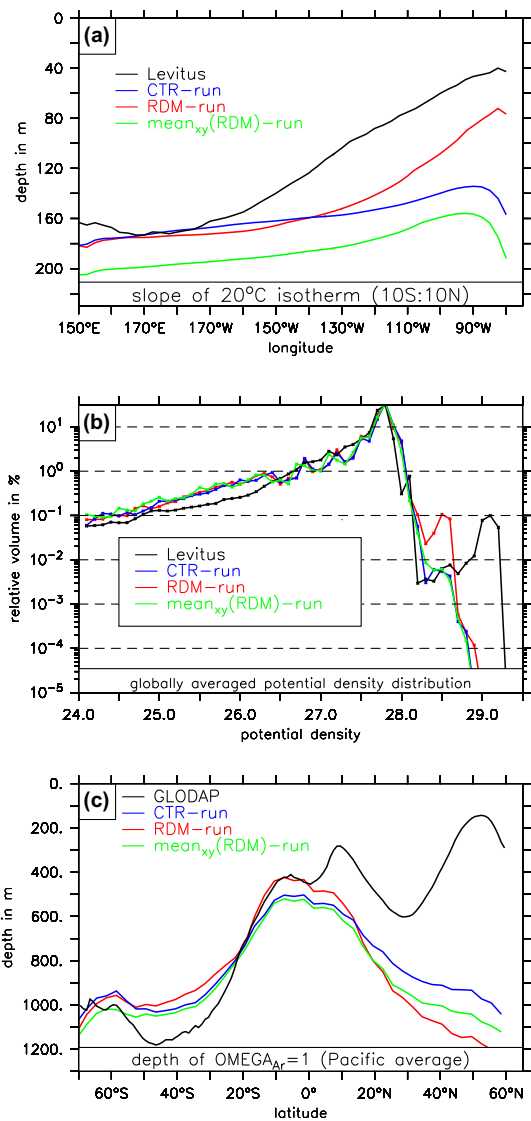


Fig. 8. (a) Slope of the Pacific 20°C isotherm averaged over 10°S to 10°N. (b) Globally averaged potential density distribution given in relative volume. Note the logarithmic y-axis. (c) Depth of aragonite saturation horizon ($\Omega_{Ar} = 1$) averaged over the Pacific. The different model runs are indicated in the panels. Observational data were taken from the Levitus climatology (Levitus, 1994) for panels a, b and the preindustrial GLODAP data set (Key et al., 2004) for panel c.

yr in the RDM-run and 61 GtC/yr in the $\text{mean}_{xy}(\text{RDM})$ -run. All three values are on the upper end of estimates (46–60 GtC/yr) provided by Carr et al. (2006) and Behrenfeld et al. (2006).

It should be noted that the simulated response of PP to changes in nutrient supply and SST may strongly depend on the complexity and parameters of the ecosystem model. A recent study by Taucher and Oschlies (2011) showed that, for example, the temperature sensitivity of the microbial loop can outweigh the effects of enhanced stratification and weaker nutrient upwelling. The largest PP changes in our model simulation (RDM-run–CTR-run) occur at the equator and coincide with the largest changes in SST. Given the fact that fast remineralization through the microbial loop is not included in our Earth system model it must be kept in mind that the PP response to the new mixing parametrization may look different using a different ecosystem model.

So far, topography-enhanced diapycnal mixing turns out to have a considerable impact on water mass ventilation, low-latitude upwelling and PP. Thus, we can expect it to have an effect on Oxygen Minimum Zones (OMZ). In our analysis we define the OMZ by oxygen concentrations lower than $90 \mu\text{mol/kg}$. Fig. 6c, d indicate the reduction in the OMZ thickness as well as the changes in the OMZ extension that is caused by applying the RDM. In the overall effect the OMZ thickness is reduced by several hundred meters over large parts of the Pacific and the Indian Ocean. Close to the North American continent the reduction rates reach 1000–2200 m at some locations. In the central North Pacific the northernmost extent of the OMZ is shifted southward by up to 20° . The southern boundary of the OMZ moves several degrees to the north in the Indian Ocean and the South Pacific. This erosion of the OMZ is accomplished by the faster ventilation of the deeper water layers from the south that increases the oxygen concentration of the upwelling waters. The near surface waters are characterized by a slight thickening of the OMZ. Here, it is the intensified PP that leads to more oxygen-consuming remineralization at depths of around 200–600 m. Overall, the volume of waters with an O_2 concentration lower than $90 \mu\text{mol/kg}$ ($10 \mu\text{mol/kg}$) decreases by 32% (11%) whereas the globally averaged O_2 concentration rises by 10%.

Accounting only for heterogeneity effects, the reduction in OMZ thickness and extension is slightly smaller. However, anomalies generated by the spatially-heterogeneous distribution of mixing

(RDM-run– $\text{mean}_{xy}(\text{RDM})$ -run) amount to a 22% (10%) decrease in the volume of waters with an O_2 concentration lower than $90 \mu\text{mol/kg}$ ($10 \mu\text{mol/kg}$).

The evolution of suboxic waters in response to enhanced diapycnal mixing are in good agreement with a study by Oschlies et al. (2008) that found OMZ volume to be a function of ventilation and the drawdown of carbon by PP (and its subsequent remineralization). They showed that increased stratification can lead to a decrease in the volume of suboxic waters which is qualitatively in line with the findings of Gnanadesikan et al. (2007). However, if PP is strengthened (as in Oschlies et al. (2008) through a coupling of carbon drawdown to atmospheric pCO_2) the increased oxygen demand for remineralization can preponderate the effect of reduced entrainment of “old” waters. The spatially-heterogeneous response of the OMZ thickness in our model runs is a manifestation of this mechanism.

With regard to our results it must be emphasized that the representation of the OMZ is rather poor in the LOVECLIM model. A minimum requirement for a reasonable representation of the OMZ is a horizontal resolution that is capable of reproducing the equatorial current system. This cannot be achieved with the LOVECLIM $3^\circ \times 3^\circ$ resolution. As shown in Fig. 6c, d, the mean extension of the OMZ (based on observational data provided by the World Ocean Atlas (Garcia et al., 2006)) cannot be reproduced. It is largely overestimated in the South Pacific and underestimated in the North Pacific. Therefore, above results need to be judged with caution even though the mechanisms behind them are qualitatively consistent with previous studies.

5.3. Changes in model biases

The global changes in overturning, density distribution, winds and biogeochemical tracers raise the question to what extent the topography-enhanced mixing scheme can improve the model's performance with respect to observations.

Fig. 7 shows the mean vertical density gradient in the upper 600 m for the control run, the RDM-run, the $\text{mean}_{xy}(\text{RDM})$ -run and the Levitus climatology (Levitus, 1994). Compared to observations, the stratification maximum in the control run is too low and in case of the tropical regions (Fig. 7b) too strong. The RDM clearly

Table 1

Root-mean-square model bias for the control run, the RDM-run and the $\text{mean}_{xy}(\text{RDM})$ -run for tracers indicated in the first column and depth levels indicated in the second column. Biases in potential temperature and salinity were calculated using the Levitus climatology (Levitus, 1994). For oxygen and phosphate data from World Ocean Atlas (Garcia et al., 2006) were taken. DIC data was taken from the GLODAP preindustrial data set (Key et al., 2004).

| Tracer | Depth | CTR-run | RDM-run | $\text{Mean}_{xy}(\text{RDM})$ -run |
|----------------------------------|------------------|---------|---------|-------------------------------------|
| Potential temperature [K] | 0–100 m | 2.878 | 2.568 | 2.993 |
| | 100–1000 m | 2.687 | 2.675 | 3.078 |
| | 1000–5500 m | 1.130 | 1.151 | 1.133 |
| | Total (0–5500 m) | 1.742 | 1.732 | 1.909 |
| Salinity [psu] | 0–100 m | 0.927 | 0.848 | 0.885 |
| | 100–1000 m | 0.463 | 0.444 | 0.459 |
| | 1000–5500 m | 0.134 | 0.152 | 0.146 |
| | Total (0–5500 m) | 0.308 | 0.299 | 0.306 |
| Oxygen [$\mu\text{mol/kg}$] | 0–100 m | 20.82 | 21.18 | 22.80 |
| | 100–1000 m | 66.92 | 69.41 | 69.15 |
| | 1000–5500 m | 56.61 | 46.91 | 54.28 |
| | Total (0–5500 m) | 58.42 | 52.26 | 57.34 |
| Phosphate [$\mu\text{mol/kg}$] | 0–100 m | 0.355 | 0.354 | 0.374 |
| | 100–1000 m | 0.578 | 0.604 | 0.604 |
| | 1000–5500 m | 0.290 | 0.322 | 0.309 |
| | Total (0–5500 m) | 0.374 | 0.402 | 0.395 |
| DIC [$\mu\text{mol/kg}$] | 0–100 m | 46.62 | 44.53 | 47.44 |
| | 100–1000 m | 71.27 | 75.10 | 72.97 |
| | 1000–5500 m | 41.01 | 45.78 | 43.04 |
| | Total (0–5500 m) | 49.71 | 53.87 | 51.53 |

rectifies the stratification bias in the upper 200 m. Most of this correction is achieved through a better representation of the equatorial upwelling. The described decrease (increase) in SST (SSS) in low latitudes provides a significant reduction in the model's bias compared to the Levitus climatology. Clearly, this improvement can be attributed to the spatial heterogeneity of mixing as it is most pronounced in the RDM-run whereas the mean_{xy} (RDM)-run provides only a small rectification.

The Southern Ocean warming largely implies an impairment of the model's performance. Only around the Ross and the Weddell Seas is the bias decreased compared to the Levitus climatology. We speculate that the coarse resolution of the ocean component of LOVECLIM results in an inadequate representation of deep and bottom water formation regions leading to a warming that is insufficiently constrained. Fig. 7c indicates that the gain in stratification in the upper 100 m of the Southern Ocean due to the RDM increases the model bias significantly.

The eastward shift in the upwelling leads to a considerably better reproduction of the slope of the 20°C isotherm in the equatorial

Pacific in the RDM-run (Fig. 8a) – which is a crucial feature for tropical climate dynamics. The use of simply higher vertical mixing that does not account for any spatial distribution apparently increases the bias in the representation by lowering the 20°C isotherm while conserving the insufficient slope in the eastern equatorial Pacific observed in the CTR-run.

Easterly winds over the equatorial Pacific are 1–6 m/s too weak in the control run compared to the ECMWF reanalysis data (Kallberg et al., 2004). The strengthening of the equatorial easterlies by 0.5–1 m/s in the RDM-run reduces the wind speed biases (not shown).

The representation of bottom water masses is improved by the RDM (Fig. 8b). The control run and the mean_{xy} (RDM)-run are lacking in water masses with a potential density of $>28.2 \text{ kg/m}^3$. While still subject to too low bottom water densities, the heterogeneity effect of topography-enhanced mixing scheme increases the proportion of the highest density class appreciably (factor 10). This leads to a better agreement with respect to the shape of the observed density distribution.

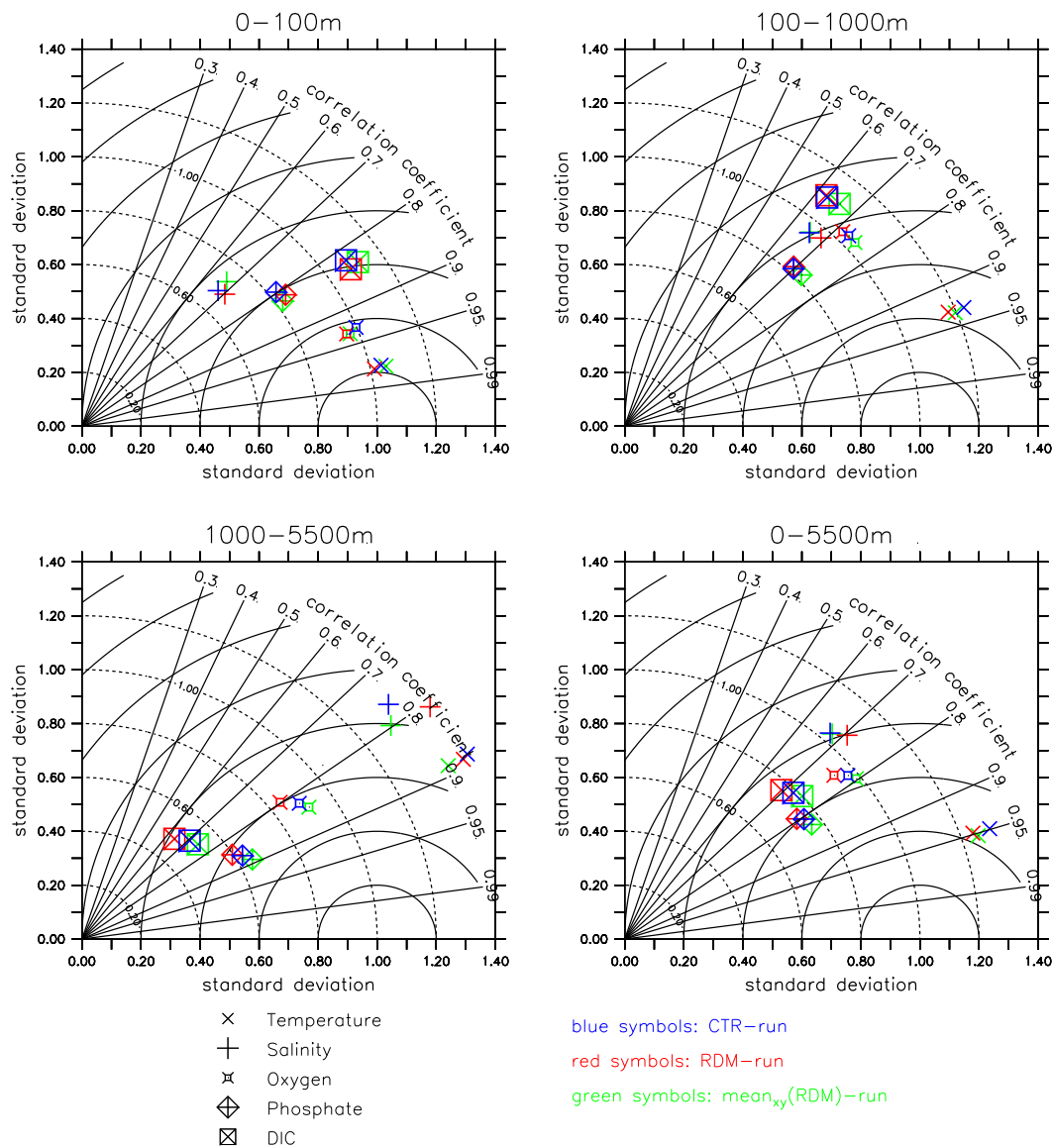


Fig. 9. Taylor diagram (Taylor, 2001) for model performance for annual mean temperature, salinity, oxygen, phosphate and DIC for the control run (blue symbols), the RDM-run (red symbols) and the mean_{xy} (RDM)-run (green symbols). Depth levels as indicated in the panels. Data were compared with Levitus climatology for temperature and salinity and with World Ocean Atlas for oxygen and phosphate (Garcia et al., 2006). For comparison with DIC, the preindustrial GLODAP data set was used. (For interpretation of the references to colour in this figure legend, the reader is referred to the web version of this article.)

Table 1 provides a summary over the model biases for the control run, the RDM-run and the mean_{xy} (RDM)-run for annual mean values of potential temperature, salinity, oxygen, phosphate and DIC respectively for different depth levels. Fig. 9 evaluates the performance for these variables in a Taylor diagram (Taylor, 2001). The near surface representation of temperature and salinity is slightly improved by RDM. This rectification which is mostly achieved in the equatorial regions cannot be explained by simply larger mixing but appears to be an effect of the spatial heterogeneity.

The enhanced ventilation of the deep ocean in the RDM-run reduces the root mean square model bias with respect to observations. Only the North Pacific constitutes an exception here. Yet in the control run using a simple depth-dependent diapycnal mixing the model is not capable of reproducing the OMZ in the North Pacific that is centered around a water depth of 1000 m. The strengthening in ventilation and the associated oxygen increase worsens the model's performance in this region. The erosion of the OMZ in the equatorial regions helps to rectify the deviation from the observed oxygen distribution. In particular in the eastern tropical Pacific the bias in OMZ thickness is reduced by up to 50%. A similar behavior is observed for the representation of aragonite saturation depth (Fig. 8c). DIC concentrations in the RDM-run are reduced in the deep North Pacific in line with increased oxygen and decreased water mass ages (Fig. 5a, c). This increases the bias in the representation of aragonite saturation depth compared to the control run. However, a slight improvement is visible for the southern tropical Pacific.

Overall, changes in model performance given as 3-dimensional pattern correlation and standard deviation with respect to 3-dimensional observations in Fig. 9 are relatively small using the different diapycnal mixing schemes. No consistent improvements or impairments can be identified in the Taylor diagrams.

Finally it needs to be emphasized that our evaluation of the model's performance can only be regarded as a preliminary estimate. Changing one parametrization in the model might require a thorough optimization ("tuning") of other parametrizations in order to achieve the best possible model performance. For example, the parametrization of downsloping currents in the standard version of our Earth system model was tuned in combination with the vertical mixing profile to ensure an optimal water mass representation. Repeating this time-consuming optimization process including the RDM would be far beyond the scope of the present study. Thus it is not clear to what extent the RDM is running in its optimal parameter range. Furthermore, an intrinsic problem of studying biogeochemical effects of a new mixing scheme in a coupled Earth system model is the long spin-up time of >3000 model years. Currently this can only be accomplished with relatively low model resolution and a reduction in complexity. As a corollary, the representation of many features that require high resolution and/or high complexity such as for example the Oxygen Minimum Zones and the spatial distribution of primary production is rather poor. The response of these features to changes in vertical mixing is therefore difficult to assess and might be very different in a –hypothetical– model study with higher complexity and better resolution.

6. Conclusions

Our results indicate that topography-enhanced mixing has a noticeable and global impact on ocean and atmospheric circulation as well as marine biogeochemistry. In our simulation, the increased and patchily-distributed diapycnal mixing results in a weakening of stratification that is associated with a strengthening of the deep overturning cell and of the equatorial upwelling. Separating the

effects of spatially-heterogeneous mixing and simply larger mixing values reveals that about 50% of the increase in overtuning can be attributed to the heterogeneity effect of the new mixing scheme. The increase in equatorial upwelling leads to a significant cooling of the low latitudes whereas the strengthening of the deep overturning cell is responsible for a warming of the Southern Ocean. These changes in surface temperature trigger atmospheric responses that in turn have a feedback on the ocean. The strengthening and the eastward shift in the equatorial upwelling in the Pacific results in a stronger Walker circulation which further increases the equatorial Ekman divergence and thus upward flow of waters. The decreasing meridional temperature gradient in the southern hemisphere leads to a weakening of the westerlies around 40°S which seems to provide a negative feedback for the strengthening of the ACC in our simulation.

Ocean ventilation is significantly improved through the spin-up of the deep overturning cell. Accordingly water mass ages drop by several hundred years in the deep North Pacific and the deep Indian Ocean whereas oxygen concentrations increase in the deep ocean. Globally, the volume of the Oxygen Minimum Zone is reduced by about 32%. Furthermore, the increase and shift in equatorial upwelling and the strengthening in near-surface Southern Ocean stratification have a bearing on the nutrient availability in the low and mid-latitudes. Primary production is strongly enhanced near the equator and reduced in the subtropical regions. Model biases in near-surface temperature and salinity are reduced by the topography-enhanced mixing in low latitudes. The warming of the Southern Ocean seems to be insufficiently constrained which leads to an impairment of the model's performance.

Finally our results indicate that the atmospheric feedback and the sea ice response can alter the changes induced by the topography-catalysed mixing. This places emphasis on the importance of a coupled model approach for reliably assessing the global effects of diapycnal mixing parametrizations.

Acknowledgements

T. Friedrich is supported by the National Science Foundation under grant number AGS-0902551. T. Decloedt is funded by National Science Foundation grant OCE-0961262. A. Timmermann is supported by the Japan Agency for Marine-Earth Science and Technology (JAMSTEC) through its sponsorship of the International Pacific Research Center. Comments from Andreas Oschlies and two anonymous reviewers are gratefully acknowledged. This is International Pacific Research Center publication 789 and School of Ocean and Earth Science and Technology publication 8163.

References

- Aucan, J., Merrifield, M.A., 2008. Boundary mixing associated with tidal and near-inertial internal waves. *J. Phys. Oceanogr.* 38, 1238–1252.
- Aucan, J., Merrifield, M.A., Luther, D.S., Flament, P., 2006. Tidal mixing events on the deep flanks of Kaena Ridge, Hawaii. *J. Phys. Oceanogr.* 36, 1202–1219.
- Behrenfeld, M.J., O'Malley, R.T., Siegel, D.A., McClain, C.R., Sarmiento, J.L., Feldman, G.C., Milligan, A.J., Falkowski, P.G., Letelier, R.M., Boss, E.S., 2006. Climate-driven trends in contemporary ocean productivity. *Nature* 444, 752–755.
- Brovkin, V., Ganopolski, A., Svirezhev, Y., 1997. A continuous climate-vegetation classification for use in climate-biosphere studies. *Ecol. Modell.* 101, 251–261.
- Bryan, K., Lewis, L., 1979. A water mass model of the world ocean. *J. Geophys. Res.* 84, 2503–2517.
- Carr, M.-E. et al., 2006. A comparison of global estimates of marine primary production from ocean color. *Deep Sea Res. Part II* 53 (5–7), 741–770.
- Decloedt, T., Luther, D.S., 2010. On a simple empirical parameterization of topography-catalysed diapycnal mixing in the abyssal ocean. *J. Phys. Oceanogr.* 40, 487–508.
- Emile-Geay, J., Madec, G., 2009. Geothermal heating, diapycnal mixing and the abyssal circulation. *Ocean Sci.* 5, 203–217.
- Eriksen, C.C., 1998. Internal wave reflection and mixing at Fieberling Guyot. *J. Geophys. Res.* 103, 2977–2994.

- Ferron, B., Mercier, H., Speer, K., Gargett, A., Polzin, K., 1998. Mixing in the Romanche Fracture Zone. *J. Phys. Oceanogr.* 28, 1929–1945.
- Fichefet, T., Morales Maqueda, M.A., 1997. Sensitivity of a global sea ice model to the treatment of ice thermodynamics and dynamics. *J. Geophys. Res.* 102 (C6), 12609–12646.
- Fichefet, T., Morales Maqueda, M.A., 1999. Modelling the influence of snow accumulation and snow-ice formation on the seasonal cycle of the Antarctic sea-ice cover. *Clim. Dynam.* 15 (4), 251–268.
- Garcia, H.E., Locarnini, R.A., Boyer, T.P., Antonov, J.I., 2006. World Ocean Atlas 2005. NOAA Atlas NESDIS 63, US Government Printing Office, Washington, D.C., Ch. Dissolved Oxygen, Apparent Oxygen Utilization, and Oxygen Saturation, 342 pp.
- Gnanadesikan, A., Slater, R.D., Gruber, N., Sarmiento, J.L., 2002. Oceanic vertical exchange and new production: a comparison between models and observations. *Deep Sea Res. Part II* 49 (1–3), 363–401.
- Gnanadesikan, A., Dunne, J.P., Key, R.M., Matsumoto, K., Sarmiento, J.L., Slater, R.D., Swathi, P.S., 2004. Oceanic ventilation and biogeochemical cycling: understanding the physical mechanisms that produce realistic distributions of tracers and productivity. *Global Biogeochem. Cycles* 18 (4), GB4010.
- Gnanadesikan, A., Russell, J.L., Zeng, F., 2007. How does ocean ventilation change under global warming. *Ocean Sci.* 3, 43–53.
- Goosse, H., Deleersnijder, E., Fichefet, T., England, M., 1999. Sensitivity of a global coupled ocean-sea ice model to the parameterization of vertical mixing. *J. Geophys. Res.* 104 (C6), 13681–13695.
- Goosse, H., Brovkin, V., Fichefet, T., Haarsma, R., Huybrechts, P., Jongma, J., Mouchet, A., Selten, F., Barriat, P.-Y., Campin, J.-M., Deleersnijder, E., Driesschaert, E., Goelzer, E., Janssens, I., Loutre, M.-F., Morales Maqueda, M.A., Opsteegh, T., Mathieu, P.-P., Munhoven, G., Pettersson, E.J., Renssen, H., Roche, D.M., Schaeffer, M., Tartinville, B., Timmermann, A., Weber, S.L., 2010. Description of the Earth system model of intermediate complexity LOVECLIM version 1.2. *Geophys. Model Dev.* 3, pp. 603–633.
- Gregg, M.C., 1987. Diapycnal mixing in the thermocline – a review. *J. Geophys. Res.* 92, 5249–5286.
- Gregg, M.C., Sanford, T.B., 1980. Signatures of mixing from the Bermuda Slope, the Sargasso Sea and the Gulf-Stream. *J. Phys. Oceanogr.* 10, 105–127.
- Griesel, A., 2005. Modeling large-scale ocean circulation: the role of mixing location and meridional pressure gradients for the Atlantic Meridional Overturning Circulation. Ph.D. Thesis, University of Potsdam.
- Hasumi, H., Sugimoto, N., 1999. Effects of locally enhanced vertical diffusivity over rough bathymetry on the world ocean circulation. *J. Geophys. Res.* 104, 23367–23374.
- Huang, R.X., Jin, X.Z., 2002. Deep circulation in the South Atlantic induced by bottom-intensified mixing over the midocean ridge. *J. Phys. Oceanogr.* 32, 1150–1164.
- Jayne, S.R., 2009. The impact of abyssal mixing parameterizations in an Ocean General Circulation Model. *J. Phys. Oceanogr.* 39, 1756–1775.
- Jayne, S.R., Laurent, L.C.S., 2001. Parameterizing tidal dissipation over rough topography. *Geophys. Res. Lett.* 28, 811–814.
- Kallberg, P., Simmons, S., Uppala, S., Fuentes, M., 2004. The ERA-40 archive. Tech. rep., ECMWF, ERA-40 Project Report Series No. 17.
- Katsman, C.A., 2006. Impacts of localized mixing and topography on the stationary abyssal circulation. *J. Phys. Oceanogr.* 36, 1660–1671.
- Key, R.M., Kozyr, A., Sabine, C.L., Lee, K., Wanninkhof, R., Bullister, J.L., Feely, R.A., Millero, F.J., Mordy, C., Peng, T.-H., 2004. A global ocean carbon climatology: results from GLODAP. *Global Biogeochem. Cycles* 18, GB4031.
- Klymak, J.M., Moum, J.N., Nash, J.D., Kunze, E., Girton, J.B., Carter, G.S., Lee, C.M., Sanford, T.B., Gregg, M.C., 2006. An estimate of tidal energy lost to turbulence at the Hawaiian Ridge. *J. Phys. Oceanogr.* 36, 1148–1164.
- Koch-Larrouy, A., Madec, G., Bouruet-Aubertot, P., Gerkema, T., Bessieres, L., Molcard, R., 2007. On the transformation of Pacific Water into Indonesian throughflow water by internal tidal mixing. *Geophys. Res. Lett.*, 34.
- Kunze, E., Sanford, T.B., 1996. Abyssal mixing: where it is not. *J. Phys. Oceanogr.* 26, 2286–2296.
- Kunze, E., Firing, E., Hummon, J.M., Chereskin, T.K., Thurnherr, A.M., 2006. Global abyssal mixing inferred from lowered ADCP shear and CTD strain profiles. *J. Phys. Oceanogr.* 36, 1553–1576.
- Laurent, L.C., Simmons, H.L., Jayne, S.R., 2002. Estimating tidally driven mixing in the deep ocean. *Geophys. Res. Lett.*, 29.
- Ledwell, J.R., St. Laurent, L.C., Girton, J.B., Toole, J.M., 2011. Diapycnal mixing in the Antarctic circumpolar current. *J. Phys. Oceanogr.* 41, 241–246.
- Levine, M.D., Boyd, T.J., 2006. Tidally forced internal waves and overturns observed on a slope: results from HOME. *J. Phys. Oceanogr.* 36, 1184–1201.
- Levitus, S., 1994. Climatological Atlas of the World Ocean. Tech. rep., NOAA Prof. Paper 13.
- Lukas, R., Santiago-Mandujano, F., Bingham, F., Mantyla, A., 2001. Cold bottom water events observed in the Hawaii ocean time-series: implications for vertical mixing. *Deep Sea Res. Part I* 48, 995–1021.
- Marshall, D.P., Garabato, A.C.N., 2008. A conjecture on the role of bottom-enhanced diapycnal mixing in the parameterization of geostrophic eddies. *J. Phys. Oceanogr.* 38, 1607–1613.
- Mellor, G., Yamada, T., 1982. Development of a turbulence closure model for geophysical fluid problems. *Rev. Geophys. Space Phys.* 20, 851–875.
- Menviel, L., Timmermann, A., Mouchet, A., Timm, O., 2008a. Climate and marine carbon cycle response to changes in the strength of the southern hemispheric westerlies. *Paleoceanography* 23. doi:10.1029/2008PA001604.
- Menviel, L., Timmermann, A., Mouchet, A., Timm, O., 2008b. Meridional reorganization of marine and terrestrial productivity during Heinrich events. *Paleoceanography* 23. doi:10.1029/2007PA001445.
- Müller, P., Xu, N., 1992. Scattering of oceanic internal gravity-waves off random bottom topography. *J. Phys. Oceanogr.* 22, 474–488.
- Munk, W., Wunsch, C., 1998. Abyssal recipes II: energetics of tidal and wind mixing. *Deep Sea Res. Part I* 45, 1977–2010.
- Nash, J.D., Kunze, E., Toole, J.M., Schmitt, R.W., 2004. Internal tide reflection and turbulent mixing on the continental slope. *J. Phys. Oceanogr.* 34, 1117–1134.
- Nikurashin, M., Ferrari, R., 2010. Radiation and dissipation of internal waves generated by geostrophic motions impinging on small-scale topography: application to the Southern Ocean. *J. Phys. Oceanogr.* 40, 2025–2042.
- Okazaki, Y., Timmermann, A., Menviel, L., Harada, N., Abe-Ouchi, A., Chikamoto, M.O., Mouchet, A., Asahi, H., 2010. Deep water formation in the North Pacific during the last glacial termination. *Science* 329, 200–204.
- Oschlies, A., Schulz, K.G., Riebesell, U., Schmittner, A., 2008. Simulated 21st century's increase in oceanic suboxia by CO₂-enhanced biotic carbon export. *Global Biogeochem. Cycles* 22, GB4008.
- Palmer, M.D., Garabato, A.C.N., Stark, J.D., Hirschi, J.J.M., Marotzke, J., 2007. The influence of diapycnal mixing on quasi-steady overturning states in the Indian Ocean. *J. Phys. Oceanogr.* 37, 2290–2304.
- Polzin, K., 1992. Observations of turbulence, internal waves and background flows: an inquiry into relationships between scales of motion. Ph.D. thesis, MIT-WHOI Joint Program in Oceanography.
- Polzin, K., 2004. Idealized solutions for the energy balance of the finescale internal wave field. *J. Phys. Oceanogr.* 34, 231–246.
- Polzin, K., Firing, E., 1997. Estimates of diapycnal mixing using LADCP and CTD data from I8S. *Int. WOCE Newsl.* 29, 39–42.
- Polzin, K., Toole, J.M., Schmitt, R.W., 1995. Finescale parameterizations of turbulent dissipation. *J. Phys. Oceanogr.* 25, 306–328.
- Polzin, K.L., Toole, J.M., Ledwell, J.R., Schmitt, R.W., 1997. Spatial variability of turbulent mixing in the abyssal ocean. *Science* 276, 93–96.
- Saenko, O.A., 2006. The effect of localized mixing on the ocean circulation and time-dependent climate change. *J. Phys. Oceanogr.* 36, 140–160.
- Saenko, O.A., Merryfield, W.J., 2005. On the effect of topographically enhanced mixing on the global ocean circulation. *J. Phys. Oceanogr.* 35, 826–834.
- Schmittner, A., 2005. Decline of the marine ecosystem caused by a reduction in the Atlantic overturning. *Nature* 434, 628–633.
- Schmittner, A., Galbraith, E.D., 2008. Glacial greenhouse-gas fluctuations controlled by ocean circulation changes. *Nature* 456, 373–376.
- Schmittner, A., Oschlies, A., Giraud, X., Simmons, H.L., 2005. A global model of the marine ecosystem for long term simulations: sensitivity to ocean mixing, buoyancy forcing, particle sinking and dissolved organic matter cycling. *Global Biogeochem. Cycles* 19, GB3004.
- Schmittner, A., Galbraith, E.D., Hostetler, S.W., Pedersen, T.F., Zhang, R., 2007. Large fluctuations of dissolved oxygen in the Indian and Pacific oceans during Dansgaard-Oeschger oscillations caused by variations of North Atlantic deep water subduction. *Paleoceanography* 22, PA3207.
- Simmons, H.L., Jayne, S.R., Laurent, L.C.S., Weaver, A.J., 2004. Tidally driven mixing in a numerical model of the ocean general circulation. *Ocean Modell.* 6, 245–263.
- Smith, W.H.F., Sandwell, D.T., 1997. Global sea floor topography from satellite altimetry and ship depth soundings. *Science* 277, 1956–1962.
- St. Laurent, L.C., 1999. Diapycnal advection by double diffusion and turbulence in the ocean. Ph.D. thesis, MIT-WHOI Joint Program in Oceanography.
- St. Laurent, L.C., Thurnherr, A.M., 2007. Intense mixing of lower thermocline water on the crest of the mid-Atlantic ridge. *Nature* 448, 680–683.
- Taucher, J., Oschlies, A., 2011. Can we predict the direction of marine production change under global warming? *Geophys. Res. Lett.* 38, L02603.
- Taylor, K.E., 2001. Summarizing multiple aspects of model performance in a single diagram. *J. Geophys. Res.* 106, 7183–7192.
- Thurnherr, A.M., 2006. Diapycnal mixing associated with an overflow in a deep submarine canyon. *Deep Sea Res. Part II* 53, 194–206.
- Toole, J.M., Schmitt, R.W., Polzin, K.L., Kunze, E., 1997. Near-boundary mixing above the flanks of a midlatitude seamount. *J. Geophys. Res.* 102, 947–959.
- Wanninkhof, R., 1992. Relationship between wind speed and gas exchange over the ocean. *J. Geophys. Res.* 97, 7373–7382.
- Wunsch, C., Ferrari, R., 2004. Vertical mixing, energy and the general circulation of the oceans. *Ann. Rev. Fluid Mech.* 36, 281–314.